Available online at www.sciencedirect.com
SCIENCE DIRECT®
Journal of Power Sources 124 (2003) 572–585
JOURNAL OF POWER SOURCES
www.elsevier.com/locate/jpowsour

Modeling the performance of an aluminum–air cell

Shao Hua Yang, Harold Knickle*
Department of Chemical Engineering, University of Rhode Island, Kingston, RI 02881, USA

Received 8 June 2003; accepted 29 June 2003

Abstract

A mathematical model for analysis and prediction of the performance of the aluminum–air cell has been developed. The model takes into account the kinetics of the anode, cathode, and parasitic reactions. Ohmic losses in the electrolyte and mass transfer are also taken into account. The model prediction of cell performance shows good agreement with experimental data. The mathematical model provides detailed information about cell performance for a wide range of operating and design parameters. For better cell performance, our model studies suggest the use of higher electrolyte flow rates, smaller cell gaps, higher conductivities, lower parasitic current densities and operation at moderate current density. From our analysis, we have determined that, in an aluminum air cell, only the activation and ohmic overpotential are important.

Keywords: Aluminum–air cell; Modeling; Analysis; Cell performance

1. Introduction

An aluminum–air battery system has the potential to be used to produce power to operate cars and other vehicles [1,2]. There are many parameters involved in the design and operation of the aluminum–air battery system. To optimize design and operation of an aluminum–air battery system, it is essential to develop a mathematical model that can predict the aluminum–air cell performance. In our previous paper, we briefly provided the cell performance model equations [3]. In this paper, a mathematical model for analysis and prediction of the performance of the unit cell has been developed in detail. The effects of mass transfer, migration, gas evolution, kinetics of electrodes, parasitic reaction and ohmic losses in the electrolyte are considered. By introducing selectivity, the algorithm for modeling calculations is simpler. MATLAB software programs were used for these calculations. This model will be used to predict cell performance (current density–cell voltage curve), the effect of electrolyte flow rate on current density distribution, the effect of cell gap on current density, and the effect of electrolyte conductivity on current density. It also is used to predict the effect of parasitic current on selectivity, activation overpotential and ohmic loss at different cell gaps, gas fraction variation with cell height, and the effect of gas fraction on electrolyte conductivity. The model also predicts the anode surface concentrations of OH^- and $Al(OH)_4{}^-$, and mass transfer boundary layer thickness.

2. Problem definition, geometry and assumptions

The cell is made up of two plane electrodes with cell gap (S) and height (H), where the height is much greater than the cell gap (Fig. 1 shows the geometry). The electrolyte enters from the bottom in laminar flow with developing boundary layer (i.e. the boundary layer thickness increases with height). The electrochemical reactions occur only on the electrode surfaces. No crystallization reaction occurs in the cell.

At the anode, the main reaction is

$$Al + 4OH^- \rightarrow Al(OH)_4{}^- + 3e^-.$$

The parasitic (undesired) reaction at the anode is

$$Al + 3H_2O + OH^- \rightarrow \tfrac{3}{2}H_2 + Al(OH)_4{}^-.$$

At the cathode, the reaction is

$$O_2 + 2H_2O + 4e^- \rightarrow 4OH^-.$$

* Corresponding author. Tel.: +1-401-874-5984; fax: +1-401-782-1066.
E-mail address: knickle@egr.uri.edu (H. Knickle).

0378-7753/$ – see front matter © 2003 Elsevier B.V. All rights reserved.
doi:10.1016/S0378-7753(03)00811-5

Nomenclature

A, b	empirical cathode kinetic constants
c_i	concentration of species i (mol/cm^3)
c_{i0}	surface concentration of species i (mol/cm^3)
$c_{i\mathrm{b}}$	bulk concentration of species i (mol/cm^3)
$c_{i,\mathrm{ref}}$	reference concentration of species i, in this article, $c_{i,\mathrm{ref}=}c_{i\mathrm{b}}$ (mol/cm^3)
d_{bubble}	diameter of bubbles (cm)
D_i	diffusion coefficient of species i (cm^2/s)
D_{R}	diffusion coefficient of the limiting reactant (cm^2/s)
E	empirical cathode kinetic constants
E_{01}	equilibrium potential of electrode 1 V
E_{eq}	cell equilibrium voltage (V)
F	Faraday's constant (96,500 C/eq.)
$f(y)$	gas fraction as a function of height
G	gravitational acceleration (cm/s^2)
H	electrode height (cm)
i_{a}	anode current density (mA/cm^2)
i_{av}	average current density (mA/cm^2)
i_{c}	cathode current density (mA/cm^2)
i_{m}	main anode reaction current density (mA/cm^2)
i_{m0}	exchange current density of the main anode reaction (mA/cm^2)
i_{p}	parasitic current density (mA/cm^2)
i_{p0}	exchange current density of the anode parasitic reaction (mA/cm^2)
n_{m}	electron transfer number in anode main reaction
n_{p}	electron transfer number in anode parasitic reaction
N	electron number per mol hydrogen molecule
N_{i}	flux of species i (mol/(cm^2 s))
P	pressure (dyn/cm^2)
R	ideal gas constant (J/(mol K))
R'	empirical cathode kinetic constant
R_i	reaction rate of species i (mol/(cm^3 s))
Re_y	Reynolds number as a function of y
$s_{i\mathrm{m}}$	stoichiometric coefficient of anode main reaction
$s_{i\mathrm{p}}$	stoichiometric coefficient of anode parasitic reaction
S	cell gap (cm)
$S_{\mathrm{m/p}}$	selectivity of main reaction over parasitic reaction
Sc	Schmidt number of species i in the electrolyte
t	time (s)
T	temperature (K)
u_i	mobility of species i (cm^2 mol/(J s))
v'_{b}	bubble rising velocity (cm/s)
V	fluid velocity (cm/s)
V_{cell}	cell voltage (V)
x, y	axial position (cm)
X	cathode extension
z_i	charge valence of ions i

Greek letters

α_{m}, $\gamma_{i\mathrm{m}}$	empirical anode kinetic constants
α_{p}, $\gamma_{i\mathrm{p}}$	empirical parasitic kinetic constants
δ_i	diffusion layer thickness of species i (cm)
$\delta_{i\mathrm{c}}$	diffusion layer thickness of species i due to convection (cm)
$\delta_{i\mathrm{b}}$	diffusion layer thickness of species i due to bubble effect (cm)
Φ	solution potential
Φ_1, Φ_2	electrode 1 (anode) potential and electrode 2 (cathode) potential
Φ_{a}, Φ_{b}	solution potential just outside the diffusion layer at electrode 1 (anode) and solution potential just outside the diffusion layer at electrode 2 (cathode)
η_1, η_2	overpotenial of electrode 1 (anode) and 2 (cathode)
η_{a1}	activation overpotential of electrode 1 (anode) (V)
η_{c1}	concentration over potential of electrode 1 (anode) (V)
η_{m}	activation overpotential of anode (V)
η_{p}	activation overpotential of parasitic reaction (V)
κ	conductivity of electrolyte at gas fraction $f(y)$ (S/cm)
κ_0	conductivity of electrolyte at zero gas fraction (S/cm)
μ	viscosity of electrolyte (g/(cm s))
ρ	density of electrolyte (g/cm^3)
ρ_{gas}	density of hydrogen gas (g/cm^3)

3. Fundamental equations

3.1. Transport in electrolyte solutions

The laws of transport in dilute electrolyte solutions have been known for many years and have been discussed in detail elsewhere [4]. The flux of a species due to migration in an electric field, diffusion in concentration gradient, and convection with the fluid velocity is:

$$N_i = -z_i u_i F c_i \nabla \Phi - D_i \nabla c_i + v c_i \quad (1)$$

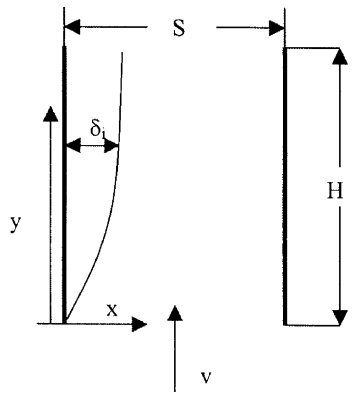

Fig. 1. Schematic of the geometry of an aluminum–air cell: δ_i, the boundary layer thickness of species i; H, cell height; S, cell gap; $H \gg S$; v, electrolyte velocity; x is measured from the electrode surface and y is measured from the cell entrance.

A material balance for a small volume element in the electrolyte is:

$$\frac{\partial c_i}{\partial t} = -\nabla N_i + R_i \tag{2}$$

In our model, there are no reactions in the electrolyte ($R_i = 0$).

To a very good approximation, the solution is electrically neutral,

$$\sum_i z_i c_i = 0, \tag{3}$$

except in the diffuse part of the double layer very close to an interface. The current density in the electrolyte solution is due to the motion of charged species:

$$i = F\sum_i z_i N_i. \tag{4}$$

These equations provide the basis for the analysis of transport in the electrolyte. The flux relation (Eq. (1)) defines transport coefficients—the mobility u_i and the diffusion coefficient D_i of an ion in a dilute solution. For flow of the electrolyte, the fluid velocity is determined from the Navier–Stokes equation:

$$\rho\left(\frac{\partial v}{\partial t} + v\nabla v\right) = \nabla p - \mu\nabla^2 v + \rho g. \tag{5}$$

Eqs. (1)–(5) can be combined to determine the concentration of each species:

$$\frac{\partial c_i}{\partial t} + v\nabla c_i = D_i\nabla^2 c_i + z_i u_i F c_i \nabla^2\Phi + z_i u_i F(\nabla c_i)\cdot\nabla\Phi. \tag{6}$$

The current density can be expressed as

$$i = -\kappa\nabla\Phi - F\sum_i z_i D_i \nabla c_i, \tag{7}$$

where

$$\kappa = F^2\sum_i z_i^2 u_i c_i \tag{8}$$

is the solution conductivity. Multiplication of Eq. (6) by $z_i F$ and addition over i gives an equation for conservation of charge:

$$-\nabla\cdot i = 0 = \kappa\nabla^2\Phi + (\nabla\kappa)\cdot\nabla\Phi + F\sum_i z_i D_i \nabla^2 c_i. \tag{9}$$

The Nernst–Einstein relation relates ionic diffusion coefficients and mobilities, at least approximately:

$$D_i = RTu_i. \tag{10}$$

We take all the diffusion coefficients to be of roughly the same magnitude, but all of them to be small in the sense that the Peclet number Pe is large:

$$Pe = \frac{UL}{D_\mathrm{R}} \tag{11}$$

where U is the characteristic velocity, L the characteristic length, and D_R is the characteristic diffusion coefficient (usually taken to be that of the limiting reactant). Note that when D_R goes to zero the Pe becomes infinite.

3.2. Electrolyte bulk medium

The region of the electrolyte outside the boundary layer is called the bulk region. It is widely known that when the Pe is large, mass transfer by convection dominates over diffusion except in a thin region, known as the diffusion layer, near the reaction surface (the electrode in this case). For large Pe (in the bulk medium), Eq. (6) reduces to

$$\frac{\partial c_i}{\partial t} + v\cdot\nabla c_i = 0. \tag{12}$$

That is, the concentration of a fluid element is constant as it moves through the solution. In most cases the appropriate solution to Eq. (12) in the bulk medium is

$$c_I = c_{I\mathrm{B}} \tag{13}$$

and all concentrations have their bulk values.

For the region outside the diffusion layer, Eq. (13) expresses the solution for the concentrations. It is still necessary to solve for the potential by means of Eq. (9), which in the bulk solution reduces to

$$\nabla\cdot\kappa\nabla\Phi = 0. \tag{14}$$

3.3. Electrolyte diffusion layer

Diffusion cannot be neglected in the layer near the reaction surface. But other simplifications are still possible. On account of the thinness of the diffusion region, effects of curvature can be neglected. We adopt the boundary layer coordinates where x is the normal distance from the surface

and y is measured along the surface from the entrance. In the diffusion layer, Eq. (6) simplifies to

$$\frac{\partial c_i}{\partial t} + v_x\frac{\partial c_i}{\partial x} + v_y\frac{\partial c_i}{\partial y} = D_i\frac{\partial^2 c_i}{\partial x^2} + z_i u_i F\left(c_i\frac{\partial^2 \Phi}{\partial x^2} + \frac{\partial c_i}{\partial x}\frac{\partial \Phi}{\partial x}\right). \quad (15)$$

We can ignore the derivatives with respect to y compared to the derivatives with respect to x. One more simplification is possible. We assume that the Schmidt number Sc is

$$Sc = \frac{\nu}{D_R} \gg 1, \quad (16)$$

where ν is the kinematical viscosity of the fluid. The Sc is on the order of 1000 for the electrolytic systems of interest here. With the assumption that the Sc is large, the diffusion layer is thin even when compared with any hydrodynamic boundary layer, which may be present, and within a two-dimensional diffusion layer the velocity components can be represented as

$$v_x = -\tfrac{1}{2}x^2\beta'(y) \quad \text{and} \quad v_y = x\beta(y), \quad (17)$$

where $\beta(y)$ is the velocity derivative at the solid wall, $\beta = \partial v_y/\partial x$ at $x = 0$, and the prime denotes the derivative with respect to y. These are the first terms in expansions of the velocity in x and satisfy the continuity equation:

$$\frac{\partial v_x}{\partial x} + \frac{\partial v_y}{\partial y} = 0. \quad (18)$$

With this approximation, the diffusion layer equation for the concentrations is

$$\frac{\partial c_i}{\partial t} - \frac{1}{2}x^2\beta' v_y\frac{\partial c_i}{\partial x} + x\beta\frac{\partial c_i}{\partial y} = D_i\frac{\partial^2 c_i}{\partial x^2} + z_i u_i F\left(c_i\frac{\partial^2 \Phi}{\partial x^2} + \frac{\partial c_i}{\partial x}\frac{\partial \Phi}{\partial x}\right). \quad (19)$$

These equations (one for each species, OH^-, $Al(OH)_4{}^-$) are to be solved along with the equation of electro-neutrality (Eq. (3)) and certain boundary conditions that are yet to be discussed.

4. Boundary conditions

4.1. Flux and concentration on the boundaries

The differential equations describing the electrolyte solution require boundary conditions. The most complex of theses concerns the kinetics of electrode reactions. A single electrode reaction can be written in symbolic form as

$$\sum_i s_{i\mathrm{m}}\mathrm{M}_i{}^{z_i} \rightarrow n_\mathrm{m}\mathrm{e}^-, \quad (20)$$

where $s_{i\mathrm{m}}$ is the stoichiometric coefficient of species i and M_i is a symbol for the chemical formula of species i. Then the boundary conditions for the concentrations in the diffusion layer are

$$c_i \rightarrow c_{i\mathrm{b}}, \quad \text{as } x \rightarrow \delta_i, \quad (21)$$

$$N_{i\mathrm{m}} = -\frac{s_{i\mathrm{m}} i_\mathrm{m}}{n_\mathrm{m} F} \quad \text{at } x = 0, \quad (22)$$

The parasitic reaction at the anode is expressed as

$$\sum_i s_{i\mathrm{p}}\mathrm{M}_i \rightarrow 0. \quad (23)$$

We obtain the stoichiometric coefficient from the reaction Eq. (23) which represents the net parasitic corrosion reaction and we obtain the electron transfer number n_p from the oxidation corrosion reaction. Then the parasitic flux of species i is

$$N_{i\mathrm{p}} = -\frac{s_{i\mathrm{p}} i_\mathrm{p}}{n_\mathrm{p} F} \quad \text{at } x = 0, \quad (24)$$

So, the total flux of species i is

$$N_{iy} = N_{i\mathrm{m}} + N_{i\mathrm{p}} = -\frac{s_{i\mathrm{m}} i_\mathrm{m}}{n_\mathrm{m} F} - \frac{s_{i\mathrm{p}} i_\mathrm{p}}{n_\mathrm{p} F} \quad \text{at } x = 0. \quad (25)$$

If we define selectivity of i_m over i_p as $S_{\mathrm{m/p}}$,

$$S_{\mathrm{m/p}} = \frac{i_\mathrm{m}}{i_\mathrm{p}} \quad (26)$$

Then Eq. (25) can be changed into

$$N_{iy} = N_{i\mathrm{m}} + N_{i\mathrm{p}} = -\left(\frac{s_{i\mathrm{m}}}{n_\mathrm{m} F} + \frac{s_{i\mathrm{p}}}{n_\mathrm{p} F S_{\mathrm{m/p}}}\right) i_\mathrm{m} \quad \text{at } x = 0. \quad (27)$$

4.2. Boundary conditions for potentials in the bulk medium

The potentials on the electrode are shown in Fig. 2. Φ_1 is the potential at the anode and Φ_2 is the potential at the cathode. The cell voltage is the difference between these two potentials

$$V_\mathrm{cell} = \Phi_2 - \Phi_1, \quad (28)$$

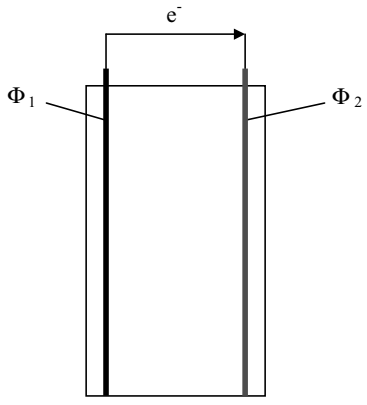

Fig. 2. Potential on the electrodes.

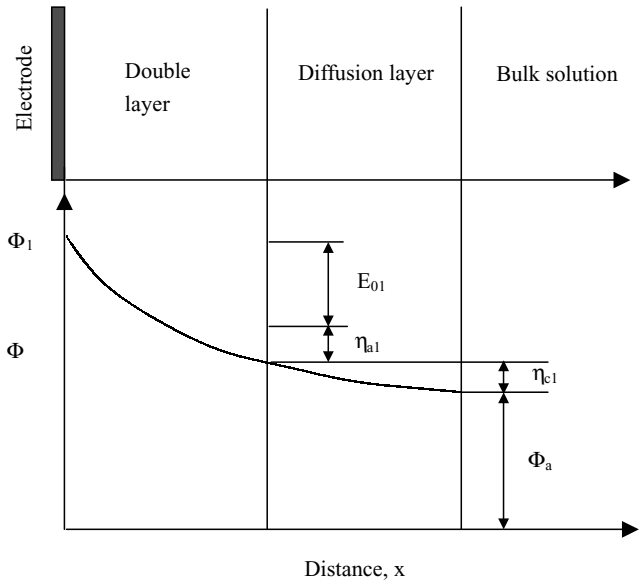

Fig. 3. Visualization of a simplified model for anodic oxidation. Φ_a is the boundary condition for the potential equation: $\nabla \cdot \kappa \nabla \Phi = 0$ in the bulk medium (adapted from [5]).

The equilibrium cell voltage (Nernst voltage) is

$$E_{eq} = E_{02} - E_{01}. \tag{29}$$

The boundary conditions are affected by the sum of both the activation and the concentration overpotential. At the anode:

$$\eta = \eta_a[i_x\,(x=0), c_{i0}, \dots] + \eta_c[i_x\,(x=0), c_{i0}, c_i, \dots]. \tag{30}$$

This equation can also be written for the cathode at $x = S$.

The boundary condition depends on the local current density flowing through the diffusion layer and the double layer. Fig. 3 visualizes a simplified model for anodic oxidation used to develop the boundary conditions for the potential Eq. (14).

The potential just outside the diffusion layer at the anode side is

$$\Phi_a = \Phi_1 - E_{01} - \eta_1, \tag{31}$$

where E_{01} is equilibrium potential of the anode, η_1 is the overpotential just outside the diffusion layer. The boundary layer includes both double layer and the diffusion layer. In an electrochemical system, there at least two electrodes, the boundary conditions for the bulk solutions at the cathode side is

$$\Phi_c = \Phi_2 - E_{02} - \eta_2. \tag{32}$$

Written under this form the boundary conditions are not practical for use because only voltage differences are of importance.

Combining Eqs. (28) and (29) with Eqs. (31) and (32) gives the potential at the anode:

$$\Phi_a = E_{eq} - V_{cell} - \eta_1 \tag{33}$$

and the potential at the cathode:

$$\Phi_c = -\eta_2. \tag{34}$$

5. Additional conditions

5.1. The concentration and activation overpotentials

For a solution with an excess of supporting electrolyte, the concentration overpotential in the electrolyte diffusion layer is [4]

$$\eta_c = \sum_i \left[\frac{s_i D_i}{n F u_i} \ln\left(\frac{c_{i0}}{c_{ib}}\right) + \frac{z_i F D_i}{\kappa_0}(c_{ib} - c_{i0}) \right]. \tag{35}$$

The surface or activation overpotential as defined above should depend only on the reaction rate and the concentrations at the electrode surface:

$$\eta_a = f[i_x\,(x=0), c_{i0}, \dots]. \tag{36}$$

This can be obtained by the modified Butler–Volmer or modified Tafel equations (see Section 5.4).

5.2. Concentration profile

The concentration profile is linearized and the whole problem is divided into two parts:

- a thin layer, called the stagnant diffusion layer with a thickness δ_i;
- the bulk of the solution where no concentration gradients exist (see Fig. 4).

5.3. Surface concentration on the anode

In the diffusion layer, the flux of OH^- and $Al(OH)_4^-$ due to the migration and diffusion, can be simplified to one dimension in the *y* direction for each component. Assuming

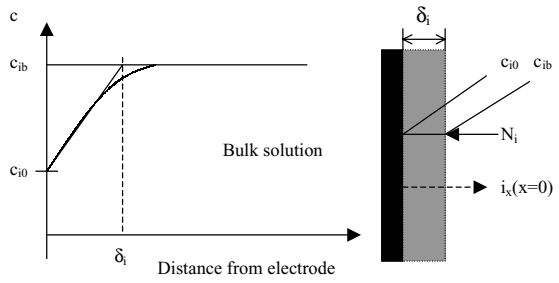

Fig. 4. The concentration profile near the electrode. The Nernst diffusion-layer is obtained by extrapolating the linear part of the concentration change to the concentration of the bulk solution.

a one dimension linear concentration profile and Ohm's law holds:

$$c_i = c_{i0} + \frac{(c_{ib} - c_{i0})x}{\delta},$$

and

$$-\nabla\Phi = \frac{i_m}{\kappa_0}.$$

Eq. (1) becomes:

$$N_i = z_i u_i F c_i \frac{i_m}{\kappa_0} - \frac{D_i(c_{ib} - c_{i0})}{\delta_i}. \quad (37)$$

and let $c_i = (c_{ib} + c_{i0})/2$, and combining Eq. (37) with Eq. (27), yields the concentration at the surface as a function of y as

$$\frac{c_{i0}}{c_{ib}} = \frac{1 + [\delta_i(i_m/\kappa_0)(F/2RT)]}{1 - [\delta_i(i_m/\kappa_0)(F/2RT)]} - \frac{[(s_{im}/n_m F) + (s_{ip}/n_p F S_{m/p})]i_m}{D_i(c_{ib}/\delta_i)[1 - \delta_i(i_m/\kappa_0)(F/2RT)]}, \quad (38)$$

where δ_i is the diffusion layer thickness for species i and is estimated by the convective electrolyte flow and the micro convection of gas evolution (see Section 5.5). δ_i is defined as the distance from the electrode where $c_i = c_{ib}$, by assuming a linear concentration profile of species i.

Eq. (38) can be written in terms of the corrosion current density, i_p, and the selectivity $S_{m/p}$:

$$\frac{c_{i0}}{c_{ib}} = \frac{1 + [\delta_i(i_p S_{m/p}/\kappa_0)(F/2RT)]}{1 - [\delta_i(i_p S_{m/p}/\kappa_0)(F/2RT)]} - \frac{[(s_{im} S_{m/p}/n_m F) + (s_{ip}/n_p F)]i_p}{D_i(c_{ib}/\delta_i)[1 - \delta_i(i_p S_{m/p}/\kappa_0)(F/2RT)]}. \quad (39)$$

Our equations to predict surface concentrations of OH^- and $Al(OH)_4^-$ are different from Chan and Savinell [6]. The difference is in the coefficients of these equations. We use Eq. (20) (main reaction) and Eq. (23) to accurately determine these coefficients. s_i/n is the stoichiometric coefficient over the electronic transfer number.

The main reaction in Eq. (20) form is

$$Al + 4OH^- - Al(OH)_4^- = 3e^-.$$

Therefore, $s_{im}/n_m = 4/3$ for OH^- and $s_{im}/n_m = -1/3$ for $Al(OH)_4^-$.

The parasitic reaction in Eq. (23) form is

$$Al + 3H_2O + OH^- - \tfrac{3}{2}H_2 - Al(OH)_4^- \rightarrow 0.$$

Therefore, $s_{ip}/n_p = 1/3$ for OH^- and $s_{ip}/n_p = -1/3$ for $Al(OH)_4^-$ where s_{ip} comes from the net parasitic (corrosion) reaction and n_p comes from the oxidation corrosion reaction.

5.4. Electrode kinetics

5.4.1. Main anode reaction kinetics

Polarization data for aluminum anodes have been reported by Rudd [7]. A simple modified Butler–Volmer form was used in this modeling work. The data of Rudd was fitted to parameters of the following expression:

$$i_m = i_{m0} \prod_i \left(\frac{c_{i0}}{c_{i,ref}}\right)^{\gamma_{im}} \left[\exp\left(\frac{\alpha_m F}{RT}\eta_m\right)\right] \quad (40)$$

where $\eta_m = \Phi_1 - \Phi_a - \eta_{c1} - E_{01}$. The subscript m stands for the main reaction.

5.4.2. Parasitic anode reaction kinetics

The parasitic reaction on aluminum can be written as

$$i_p = i_{p0} \prod_i \left(\frac{c_{i0}}{c_{i,ref}}\right)^{\gamma_{pi}} \left[\exp\left(\frac{\alpha_p F}{RT}\eta_p\right)\right], \quad (41)$$

where

$$\eta_p = \eta_{1a} + E_{01} - E_{0p}. \quad (42)$$

5.4.3. Cathode kinetics

For the porous air cathode, a modified Tafel equation was used:

$$\eta_c = a + b\log(|i_c|) + e|i_c|. \quad (43)$$

5.5. Diffusion layer thickness

The diffusion layer thickness is estimated by taking into account convection from electrolyte flow and microconvection effects from gas evolution (see also [6]).

The position dependent boundary layer thickness due to convection effects is expressed as [8]

$$\delta_{ic} = 1.08 Sc^{-1/3} Re_y^{-1/2} y^{0.95} S^{0.05}. \quad (44)$$

In a stagnant fluid, the diffusion layer thickness can be correlated to the bubble generation rate by the equation [9]:

$$\delta_{ib} = 0.0103 i_p^{-0.36}. \quad (45)$$

The combined effect of convection and microconvection on the diffusion layer thickness can be estimated as [10]

$$\delta_i = \frac{\delta_{ic}\delta_{ib}}{(\delta_{ic}^2 + \delta_{ib}^2)^{1/2}}. \quad (46)$$

A calculated value of $\delta_i(OH^-)$ at a cell voltage of 1.3 V, height of 17 cm and a cell gap of 0.2 cm is about 6.5×10^{-3} cm, 3.2% of the cell gap.

5.6. Electrolyte conductivity

The presence of the gas bubbles in the cell gap decreases the electrolyte conductivity, and this effect can be estimated by the Bruggemann equation (see also [6]):

$$\kappa(y) = \kappa_0 \left[1 - f(y)\right]^{1.5}, \quad (47)$$

where $f(y)$ is the axial position y dependent gas fraction of the electrolyte. $f(y)$ can be estimated by the following equation [11]:

$$f(y) = \frac{\rho_{\text{gas}}^{-1}}{HnFv_{\text{b}}'} \int_0^h i_{\text{p}}(y)\,\mathrm{d}y, \tag{48}$$

where v_{b}' is bubble rise velocity, n is electrons transferred/mol gas, and ρ_{gas} is gas density.

5.7. Bubble rise velocity

In a stagnant solution, after formation, a bubble rapidly accelerates to its terminal velocity, v_{b}. The value of v_{b} is determined by the balance between the buoyant raising force and the drag force. While it is easy to calculate the buoyancy force for a bubble, the drag force varies with bubble size. For small, spherical bubbles, the drag force can be calculated, and when combined with the buoyancy force, yields Stoke's law:

$$v_{\text{b}} = \frac{\rho g d_{\text{bubble}}^2}{18\mu}, \tag{49}$$

where ρ is the density of the fluid, d_{bubble} the diameter of the bubbles, and μ is the viscosity of the fluid.

If the velocity of the fluid is v, the rise velocity of the small bubble will be:

$$v_{\text{b}}' = v_{\text{b}} + v \tag{50}$$

6. Cell performance model

6.1. Cell performance model: summary

Eqs. (26), (33), (34), (38) and (40)–(46) form the set of equations for our cell performance model.

The model includes the effects of mass transfer, migration, gas evolution, and the kinetics of the electrodes. The mathematical model provides detailed information about cell performance for a wide range of operating and design parameters. In summary, the electrolyte has been broken into two regions: bulk medium and diffusion layer. If we combine the diffusion layer and double layer as one boundary layer, the cell performance of the aluminum–air cell can be modeled by the potential equation:

$$\nabla \cdot \kappa \nabla \Phi = 0.$$

boundary conditions:

$$\Phi_{\text{a}} = E_{\text{eq}} - V_{\text{cell}} - \eta_1,$$

$$\Phi_{\text{c}} = -\eta_2,$$

and additional Eqs. (38) and (40)–(46) which are used to calculate η_1 and η_2 (see Section 5). The calculation procedures are outlined in Section 6.3. We determine current density at position x and average current density of the cell at a fixed cell voltage.

6.2. Model assumptions

1. Two electrodes are in parallel.
2. The cell is sufficiently long ($H \gg S$) so that entrance effects on the cell performance curve are neglected.
3. Simple Ohm's law is used in the bulk layer to predict the potential: $-\nabla\Phi = (\Phi_{\text{a}} - \Phi_{\text{c}})/S = i_{\text{m}}/\kappa$ (one dimension).

With these assumptions, the cell performance modeling is turned into a one-dimensional problem.

6.3. Model computational algorithm

For a fixed cell voltage, the following procedures are used to calculate current density at position x and average current density of the cell:

1. Assuming a current density i_{m}, $c_{i0} = c_{i\text{b}}$ (no concentration polarization) and $\kappa = \kappa_0$ (no gas effect).
2. Calculate η_{a1} by Eq. (40), η_{a2} by Eq. (43), η_{p} by Eq. (42) and i_{p} by Eq. (41).
3. Calculate δ_i by Eqs. (44)–(46), $f(y)$ by Eq. (48), $\kappa(y)$ by Eq. (47).
4. Calculate $c_{i0}/c_{i\text{b}}$ by Eq. (38) and by estimating $\nabla\Phi(= (\Phi_{\text{a}} - \Phi_{\text{c}})/S = i_{\text{m}}/\kappa)$.
5. Recalculate η_{a1} by Eq. (40), η_{a2} by Eq. (43), η_{p} by Eq. (42) and i_{p} by Eq. (41), and calculate $S_{\text{m/p}}$ by Eq. (26).
6. Calculate voltage of the cell, V.

Calculate V by Eqs. (33) and (34) and $(\Phi_{\text{a}} - \Phi_{\text{c}})/S = i_{\text{m}}/\kappa$ (Ohm's law):

Case 1: $V > V_{\text{cell}}$, increase i_{m}, go back to step 2.
Case 2: $V < V_{\text{cell}}$, decrease i_{m}, go back to step 2.
Case 3: $V = V_{\text{cell}}$, the resulted i_{m} is the current density at position y.

7. Calculate average current density

$$i_{\text{av}} = \sum \frac{\delta y i_{\text{m}}}{H}$$

The parameters used to calculate cell performance are tabulated in Table 1.

If we determine the cathode parameters from the Yardney (AC series) cathode [12] for oxygen reduction, the coefficients in Eq. (43) listed in Table 2.

7. Model calculations

7.1. Model verification

Fig. 5 shows the model predicted cell performance curve (curve 1) compared to experimental data. The solid curves is plotted using the Algorithm in Section 6.3. The circles are experimental data at temperature of 333 K (see [6]) with electrolyte velocity of 1.7 cm/s and a cell gap of 0.14 cm. In

Table 1
Parameters used in the cell performance modeling [6]

	Parameters
Anode kinetic parameters	
Main	$i_{m0} = 13.71\,mA/cm^2$, $\alpha_m = 0.07956$, $\gamma_m = 0.5$, $E_{01} = -2.4403\,V$ (from Eq. (40))
Parasitic	$i_{p0} = 11\,mA/cm^2$, $\alpha_p = -0.0591$, $\gamma_p = 1$, $E_{0p} = 0.9058\,V$ (from Eqs. (41) and (42))
Cathode kinetic parameters	See Table 2 (from Eq. (43))
Substance physical properties	$c_{OH^-,b} = 5 \times 10^{-3}$ mol/cm^3, $D_{OH^-,b} = 5.26 \times 10^{-5}\,cm^2/s$, $c_{AlOH^-,b} = 5 \times 10^{-4}$ mol/cm^3, $D_{AlOH^-,b} = 10^{-5}\,cm^2/s$, $\rho = 1.15\,g/cm^3$, $\mu = 0.008\,g/(cm\,s)$, $\rho_{gas} = 7.32 \times 10^{-8}\,g/cm^3$, d_{bubble}[a] $= 2.6 \times 10^{-3}$ cm, $\kappa_0 = 0.8\,s/cm$
Operating conditions	Temperature = 333 K
Constants	$F = 96{,}500\,C/eq.$, $R = 8.314\,J/(mol\,K)$, $g = 980\,cm/s^2$

[a] From [9].

Table 2
Cathode kinetic parameters for the modified Tafel equation (Eq. (43))

Cathode	Kinetic parameters		
	a	*b*	*e*
AC65 Yardney (Ag)	−0.2856	−0.0316336	-6.631×10^{-4}
AC75 Yardney (CoTMPP)	−0.1945	−0.02901276	-7.402×10^{-4}
AC78 Yardney (Pt)	−0.2118	−0.0255886	-6.706×10^{-4}
Chan and Savinell	−0.29289	−0.025096	-2.03429×10^{-4}

curve 1, the cathode kinetic parameters are from Chan and Savinell. The agreement between the model and the data is good at current densities from 180 to 500 mA/cm^2.

In curve 2, the cathode kinetic parameters are from Yardney AC78. From the kinetic parameters of Yardney cathode AC78, we can see that the ohmic resistance term *e* (absolute value) is bigger than the one given by Chan and Savinell, so at higher current density, the Yardney AC78 cathode has higher polarization thus the cell voltage is lower at the same current density.

7.2. Effect of electrolyte flow rate on current density distribution

Fig. 6 shows the effect of electrolyte flow rate (velocity) on current density distribution along the cell. Because of the evolution of hydrogen gas in the electrolyte, the ohmic resistance will increase along the cell (resulting in a decrease of current density along the cell) if the electrolyte flow rate is not high enough to remove the bubbles. With increase in the electrolyte flow rate, the current distributions along the cell become closer to uniform, which suggests that operating at a high flow rate (8 cm/s), the gas effect will be alleviated.

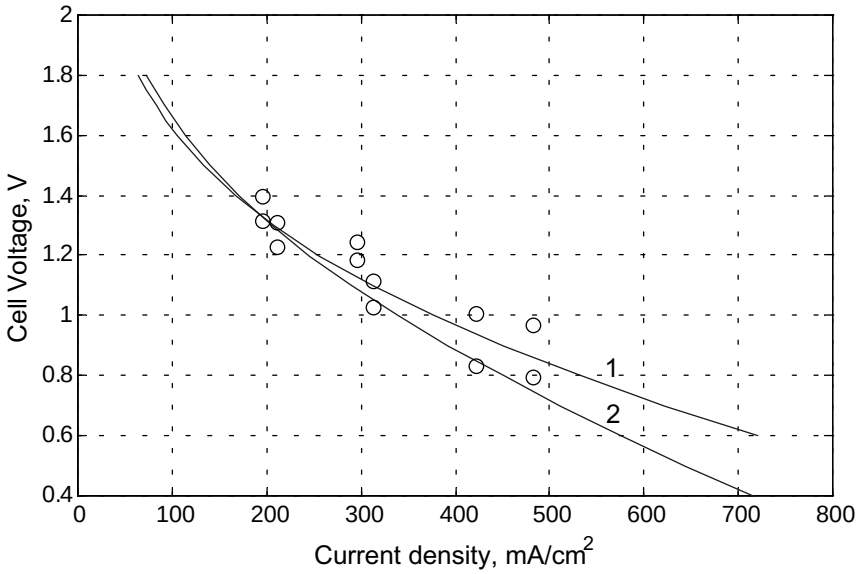

Fig. 5. Cell performance of an aluminum air cell with pure aluminum anode. Curve 1: the cathode kinetic parameters are from Chan and Savinell; curve 2: the cathode kinetic parameters are from Yardney AC78.

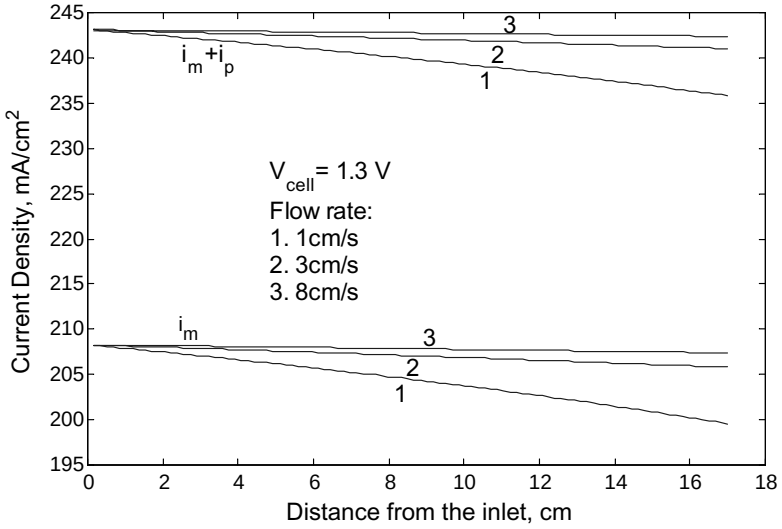

Fig. 6. Effect of flow rate on current distribution along the cell. Cell gap = 0.2 cm.

Table 3
Velocity and Reynolds number relationship

Velocity (cm/s)	*Re*
1	56
3	167
5	279
8	446
14	780
18	1003

Cell gap = 0.2 cm.

The Reynolds number (*Re*) increases with flow rate. The relationship of *Re* and velocity is tabulated in Table 3. The *Re* number indicates laminar flow over a wide range of velocities because of the narrow channel used.

7.3. Effect of cell gap on current density

The effect of cell gap on the current density at different constant voltages is shown in Fig. 7. To alleviate the effect of gas bubbles in the electrolyte, a flow rate of 8 cm/s (see Section 5.4.2) is used in our calculation. In a two plane, parallel electrodes design, with the consumption of the anode, the cell gap will increase, and thus the ohmic resistance will increase. Larger cell gap means larger ohmic resistance. At lower cell voltage, the current density is higher, and the cell gap has a greater effect on the current density.

7.4. Effect of parasitic current on selectivity–corrosion inhibitor

One of the objectives in the optimization of the cell performance is to increase the selectivity of the main current

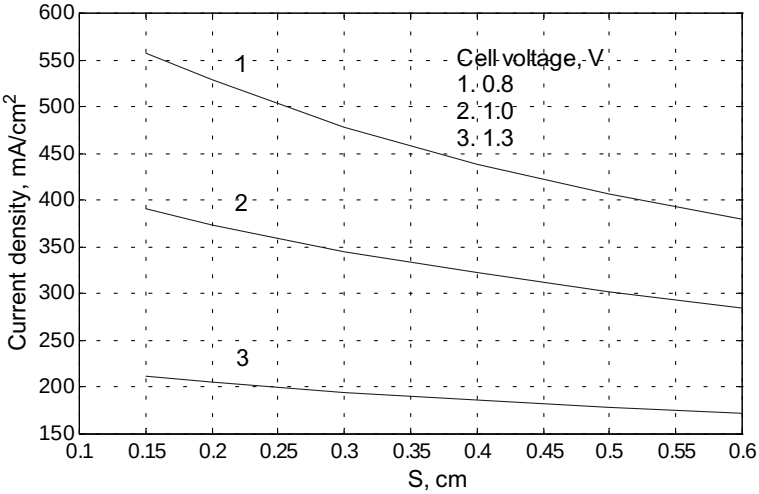

Fig. 7. Effect of cell gap on current density at different constant voltages and a electrolyte flow rate of 8 cm/s.

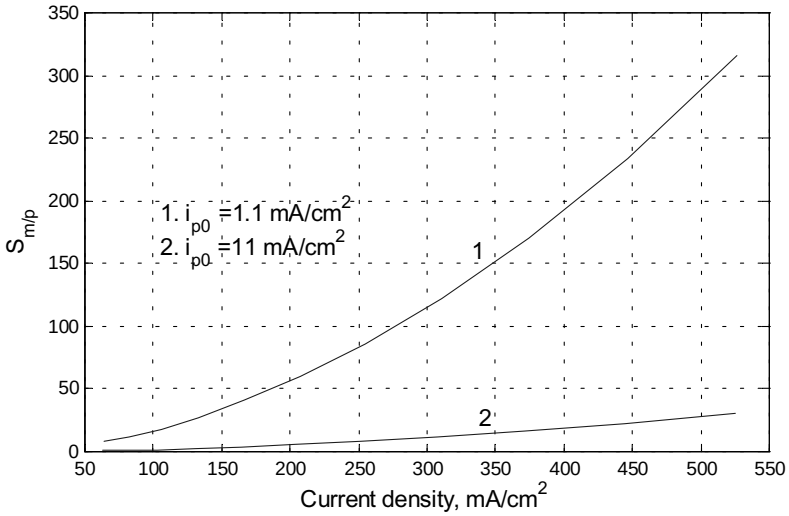

Fig. 8. Effect of corrosion current on selectivity at a flow rate of 8 cm/s and cell gap of 0.2 cm using sodium stannate as a corrosion inhibitor.

density over parasitic current density. From Fig. 8, one can see that if we can decrease parasitic current by a factor of 10, the selectivity will be much higher. In using pure aluminum, and no corrosion inhibitor addition in the electrolyte, the selectivity will be very low at low current density (main reaction) (curve 2). In the case of using aluminum alloy (Al 1199) and the additive sodium stannate (Na_2SnO_3), a corrosion inhibitor, in the electrolyte, the parasitic current will decrease by a factor of ten as we have shown in our experimental studies.

7.5. Effect of electrolyte conductivity on current density

Fig. 9 shows the effect of electrolyte conductivity on current density at different constant cell voltages. Small changes in electrolyte conductivity have significant effect on the current density. With an increase in conductivity, the current density will significantly increase in all three cases. So in the choice of the electrolyte, the conductivity will be an important factor. The specific electrolyte, its concentration and temperature all affect the conductivity of the electrolyte. A KOH aqueous solution has higher conductivity than a NaOH aqueous solution when their concentrations are equal. That is why many people choose KOH aqueous as the electrolyte. Of course, other factors should also be taken into account such as the effect of different electrolyte on the crystallization of the products and the regeneration of aluminum by the industrial Hall–Herout process.

7.6. Activation overpotential and ohmic loss at different cell gaps

Activation overpotential and ohmic loss at different cell gaps are listed in Table 4. The concentration overpotential

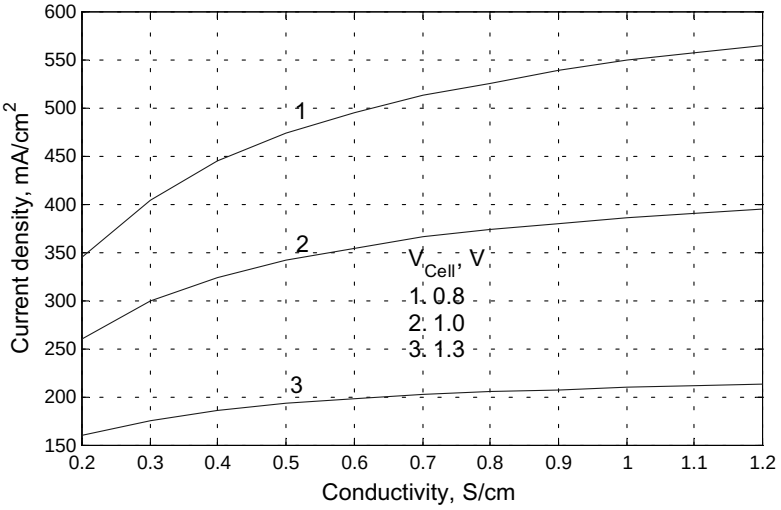

Fig. 9. Effect of conductivity on current density at different constant cell voltages at a flow rate of 8 cm/s and cell gap of 0.2 cm.

Table 4
Cell Overpotential and ohmic losses at 0.8 V and 8 cm/s velocity

Cell gap (cm)	Current density (mA/cm^2)	Activation loss (V)		Ohmic loss (V)	Total loss (V)
		Anode	Cathode		
0.2	528	1.32 (68.4%)	0.47 (24.4%)	0.14 (7.2%)	1.93 (100%)
0.4	437	1.25 (64.7%)	0.45 (23.7%)	0.23 (11.6%)	1.93 (100%)
0.6	381	1.20 (62.2%)	0.43 (22.2%)	0.30 (15.6%)	1.93 (100%)
0.8	338	1.16 (60.1%)	0.42 (21.8%%)	0.35 (18.1%)	1.93 (100%)

is not included in this table for it is very small compared with the activation overpotential and ohmic loss. At a flow rate of 8 cm/s, the effect of gas bubbles on ohmic resistance is small, the ohmic resistance is considered to be constant along the cell channel. When the cell gap increases from 0.2 to 0.8 cm, the anode overpotential decreasing from 68.4 to 60.1% (8.3% net decrease); the cathode overpotential is relatively stable, it decreases from 24.4 to 21.8% (2.6% net decrease); the ohmic loss increases from 7.2 to 18.1% (10.9% net decrease). The current density decreases from 528 to 338 mA/cm^2 (190 mA/cm^2 or 36.0% net decrease). Although at a fixed cell voltage of 0.8 V, the ohmic loss only increases 7.2–18.1%, the effect on current density is significant, 36% current density will be lost due to the increase of ohmic loss (or cell gap).

Table 5 shows overpotential and ohmic losses at two cell gaps, different cell voltages. We can see that the ohmic loss become important at higher current density (lead to the decrease of current density at the same cell voltage), and selectivity is higher at higher current density.

7.7. Gas fraction variation with cell height

Fig. 10 indicates the gas fraction variation with height in the aluminum–air cell. Calculations represented in Fig. 10 have been made when there is no additive in the electrolyte to suppress the corrosion reaction. It is clear that the volume fraction takes up a significant percentage of the channel at the exit rising from 20% for *Case 1* to as high as 40% for *Case 3*. These volume fractions cause large reductions in the cell conductivity and indicate the importance of additives under these conditions. Fig. 11 clearly depicts the importance of increasing the electrolyte velocity to sweep out the bubbles generated from the corrosion reaction. The higher velocities markedly reduce the gas volume fraction yielding higher electrolyte conductivity.

If we used a corrosion inhibitor in the calculations for Fig. 10 to reduce the exchange current density of the corrosion reaction to $i_{p0} = 1.1$ mA/cm^2 the volume fraction at a cell height of 17 cm, flow velocity of 1 cm/s, 1.3 V and 200 mA/cm^2 reduces to 0.02 from about 0.2. The additive causes a reduction by a factor of 10 in the volume fraction. Other parameters are unchanged in the corrosion kinetic equation.

7.8. Effect of gas fraction on electrolyte conductivity

Electrical conductivity calculations using the values of Fig. 10 demonstrate the reduction in electrical conductivity in the bulk electrolyte flow. The reference value for the electrolyte conductivity is 0.8 S/cm. As the gas fraction builds up with height in the three cases illustrated,

Table 5
Overpotential and ohmic losses at different cell gaps, different cell voltages and a flow rate of 8 cm/s.

Cell gap = 0.2 cm						
Voltage, V	0.4	0.6	0.8	1	1.2	1.4
i_m	932.4	715.9366	529.05	375	254.53	166
$S_{m/p}$	85.85	53.2843	31.06	16.8942	8.5507	4.0446
Anode loss	1.5289	1.4314	1.3206	1.195	1.054	0.8999
Cathode loss	0.5566	0.5098	0.4685	0.4335	0.4048	0.3822
Ohmic loss	0.2405	0.1848	0.1369	0.0975	0.0672	0.0439
Total loss	2.326	2.126	1.926	1.726	1.526	1.326
Cell gap = 0.4 cm						
Voltage, V	0.4	0.6	0.8	1	1.2	1.4
i_m	732.9783	577.7783	440.075	322.37	226.408	152.39
$S_{m/p}$	55.5849	36.3326	22.4186	12.9513	6.964	3.483
Anode loss	1.4402	1.3529	1.2535	1.1404	1.0122	0.869
Cathode loss	0.5136	0.4794	0.4485	0.4212	0.3978	0.3785
Ohmic loss	0.3722	0.2937	0.224	0.1644	0.116	0.0785
Total loss	2.326	2.126	1.926	1.726	1.526	1.326

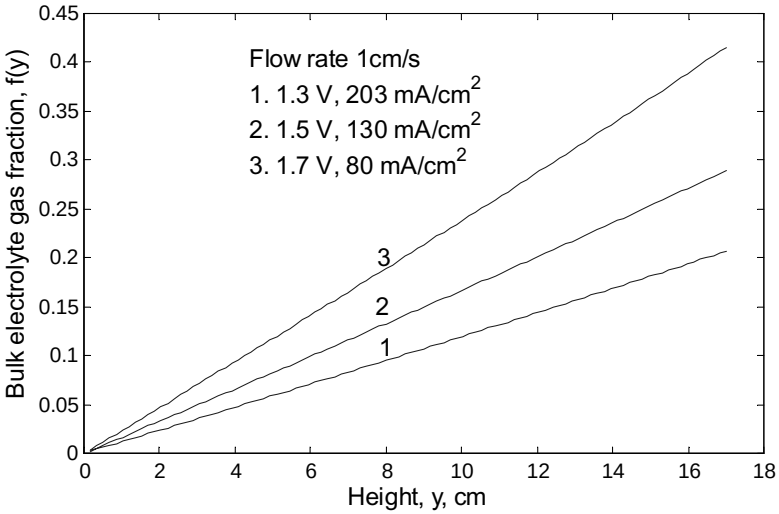

Fig. 10. The gas fraction variation with height in the aluminum–air cell at a flow rate of 1 cm/s.

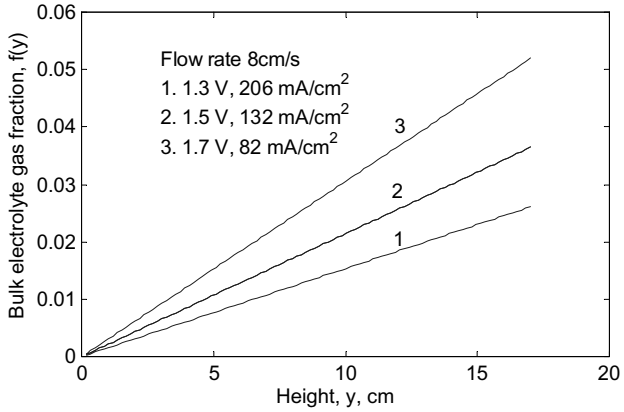

Fig. 11. The gas fraction variation with height in the aluminum–air cell at an electrolyte velocity of 8 cm/s.

the electrical conductivity is significantly reduced (Figs. 12 and 13).

7.9. Anode surface concentrations

Table 6 shows the surface concentrations on the anode at a cell height of 17 cm and $i_{p0} = 11\,\text{mA/cm}^2$. The surface concentrations of OH^- and $Al(OH)_4^-$ are similar at electrolyte velocities of 1 and 8 cm/s. At current densities between 520 and 530 mA/cm^2, the surface concentration of OH^- is 2% less than the concentration in the bulk electrolyte and the surface concentration of $Al(OH)_4^-$ is 8% larger than the concentration in the bulk electrolyte.

Table 7 shows the surface concentrations on the anode at a cell height of 17 cm and $i_{p0} = 1.1\,\text{mA/cm}^2$. The surface concentrations of OH^- and $Al(OH)_4^-$ are also similar at electrolyte velocity of 1 and 8 cm/s. At current density

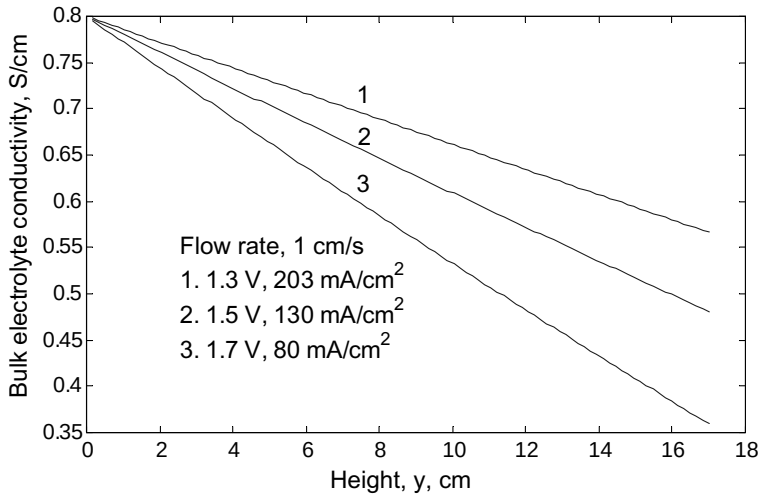

Fig. 12. The reduction in electrical conductivity in the bulk electrolyte flow at electrolyte velocity of 1 cm/s.

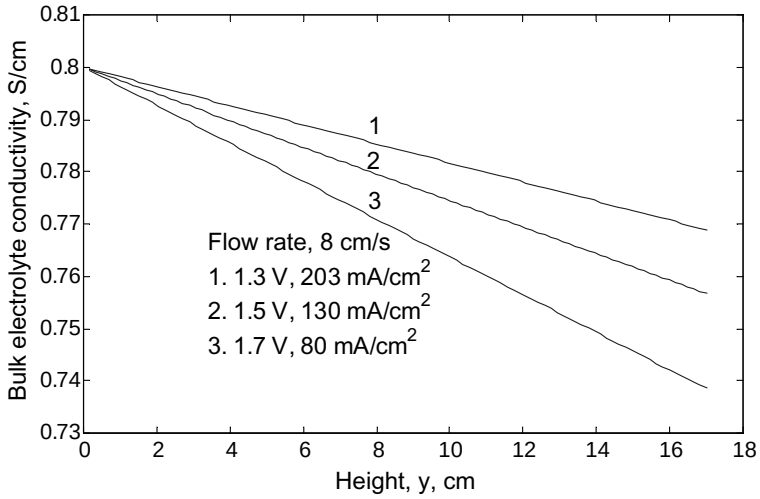

Fig. 13. The reduction in electrical conductivity in the bulk electrolyte flow at electrolyte velocity of 8 cm/s.

Table 6
The surface concentrations on the anode at cell height of 17 cm and $i_{p0} = 11\,mA/cm^2$

$v = 1$ cm/s						
Cell voltage, V	0.4	0.6	0.8	1	1.2	1.4
i_m	920	705	521	368	250	163
$S_{m/p}$	84.0154	52.0133	30.2559	16.42	8.2969	3.9179
$c_{OH,0}/c_{OH,b}$	0.9606	0.9727	0.9815	0.9879	0.99	0.995
$c_{AlOH,0}/c_{AlOH,b}$	1.1893	1.1296	1.0859	1.0543	1.033	1.019
$v = 8$ cm/s						
Cell voltage, V	0.4	0.6	0.8	1	1.2	1.4
i_m	932	716	529	374.9092	254.03	165.9951
$S_{m/p}$	85.849	53.2843	31.06	16.8942	8.5507	4.0446
$c_{OH,0}/c_{OH,b}$	0.9606	0.9723	0.9812	0.9876	0.99	0.995
$c_{AlOH,0}/c_{AlOH,b}$	1.1893	1.1317	1.0878	1.0559	1.033	1.0197

Table 7
Surface concentration at cell height of 17 cm and $i_{p0} = 1.1\,mA/cm^2$

$V = 1$ cm/s						
Cell voltage, V	0.4	0.6	0.8	1	1.2	1.4
i_m	911	703	522	371.8	253.2285	165.53
$S_{m/p}$	905.41	548.13	315.137	170.083	85.7438	40.4854
$c_{OH,0}/c_{OH,b}$	0.897	0.9318	0.9559	0.9725	0.9834	0.9903
$c_{AlOH,0}/c_{AlOH,b}$	1.502	1.3324	1.2143	1.133	1.0797	1.0457
$V = 8$ cm/s						
Cell voltage, V	0.4	0.6	0.8	1	1.2	1.4
i_m	917	707.55	524.556	372.86	253.7788	165.844
$S_{m/p}$	894.07	545.58	315.029	170.33	85.9372	40.5864
$c_{OH,0}/c_{OH,b}$	0.911	0.9393	0.9599	0.9745	0.9844	0.9908
$c_{AlOH,0}/c_{AlOH,b}$	1.4326	1.2951	1.1948	1.1236	1.075	1.0435

520–530 mA/cm^2, the surface concentration of OH^- is 4% less than the concentration in the bulk electrolyte and the surface concentration of $Al(OH)_4^-$ is 20% larger than the concentration in the bulk electrolyte. Comparing the results of Tables 6 and 7, we can see that, at high corrosion rate, the surface concentration polarization can be relieved.

8. Conclusions

We have modeled the aluminum–air cell performance using the equations we have developed in this study. The model prediction of cell performance shows good agreement with experimental data. For better cell performance,

our model studies suggest the use of higher electrolyte flow rates, smaller cell gaps, higher conductivities, lower parasitic current densities, and operation at moderate current densities. From our analysis, we have determined for relatively high flow rates high (>8 cm/s) in an aluminum air cell, the gas effect on current density distribution is small. We can also conclude that only the activation and ohmic overpotentials are important in the model calculations. Further the proper additive can increase the selectivity by a factor of 10.

References

[1] S. Yang, H. Knickle, Design and analysis of aluminum–air battery system for electric vehicles, J. Power Sources 112 (1) (2002) 162–173.
[2] S. Yang, H. Knickle, Aluminum–air electric vehicle life cycle analysis, in: Proceedings of the 202nd Meeting of the Electrochemical Society, Salt Lake City, UT, USA, 20–24 October 2002.
[3] S. Yang, H. knickle, Two-dimensional transport modeling of an aluminum–air cell, in: Proceedings of the 203rd Meeting of the Electrochemical Society, Paris, France, 27 April–2 May 2003.
[4] J. Newman, The effect of migration in laminar diffusion layers, Int. J. Heat Mass Transfer 10 (1967) 983–997.
[5] J. Deconinck, Current distributions and electrode shape changes in electrochemical systems, in: C.A. Brebbia, S.A Orszag (Eds.), Lecture Notes in Engineering, Springer-Verlag, Berlin, 1992.
[6] K.Y. Chan, R.F. Savinell, Modeling calculations of an aluminum–air cell, J. Electrochem. Soc. 138 (7) (1991) 1976–1984.
[7] E.J. Rudd, Final Report for the Department of Energy Contract, SNLA 02-8199, 1988.
[8] D.J. Pickett, Electrochemical Reactor Design, Elsevier, Amsterdam, 1979.
[9] L.J.J. Janssen, J.G. Hoogland, The effect of electrolytically evolved gas bubbles on the thickness of the diffusion layer-II, Electrochim. Acta 18 (1973) 543–550.
[10] H. Vogt, Mass transfer at gas evolving electrodes with superposition of hydrodynamic flow, Electrochim. Acta 23 (1978) 203–205.
[11] C.W. Tobias, Effect of gas evolution on current distribution and ohmic resistance in electrolyzers, J. Electrochem. Soc. 106 (9) (1959) 883.
[12] Alupower, AC78 Technical Data Sheet, September 2002 (http:/www.yardney.com).